Corrosion and Protection of Silicon Nitride Insulators in Microelectrode Array Applications

Antti Karttu, Kimmo Lahtonen, Juha Heikkilä, Jari Väliaho, Susanna Narkilahti, Jukka Lekkala, and Pasi Kallio, *Member, IEEE*

***Abstract*—In the study of the electrophysiological activity of cultured cells, the integrity of the electrical insulation layer is crucial in ensuring the reliability of microelectrode array (MEA) sensor measurements. The materials used are required to withstand the challenging culture conditions for up to several months. The commonly used silicon nitride (SiN) has been reported to corrode in cell cultures with very little attention in the scientific community. Herein, we show that plasma-enhanced chemical vapor deposited (PECVD) SiN is subject to substantial wear when in contact with different culture media, with the corrosion rate depending on the deposition temperature and media type. A chemically stable insulator is proposed and demonstrated as an alternative for SiN using thermally annealed atomic layer deposited (ALD) titanium dioxide (TiO_2) as a transparent protective layer for SiN. Electrochemical impedance spectroscopy (EIS) was successfully applied to periodically assess the integrity and thickness of the insulation layers in two different media, with profilometer measurements performed as an endpoint analysis to confirm the actual change in thickness in four solutions. ALD TiO_2 not only prevented insulator corrosion but also showed excellent cytocompatibility during a four-week culture with human embryonic stem cell (hESC)-derived neurons. The results here underline the need for addressing the corrosion of SiN insulation in MEA sensors. We believe that the integrity and results of cellular measurements can be compromised, especially when reusing MEAs. We propose the ALD TiO_2 protected insulator as a viable solution for this problem, as it increases reliability, particularly during extended cell cultures.**

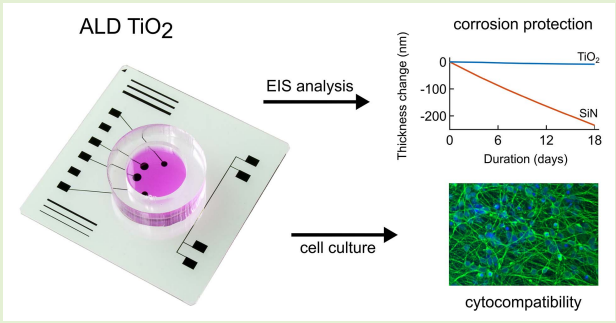

***Index Terms*—Atomic layer deposition, biosensor, corrosion, cytocompatibility, electrochemical impedance spectroscopy, MEA, microelectrode array, silicon nitride, titanium dioxide.**

I. Introduction

SINCE their introduction nearly five decades ago, microelectrode arrays (MEAs) have had a broad impact on studying the extracellular electrophysiological activity of neural and cardiac cells. The noninvasive measurement technique of field potentials enabled by surface integrated planar MEA sensors provides tools to benefit fields of developmental biology [1], [2], pathological studies [2], [3] and pharmacological research [4]–[6].

Major benefits of using MEAs include providing cultured cells with a stable proliferation platform that can be used for continuous and simultaneous monitoring of electrical activity at multiple locations without mechanically interfering with cellular functions. The spatial information attached to the recordings can be used to assess the formation, plasticity and maturation of developing networks, as well as pathological events [4]. Due to the advent of human-induced pluripotent stem cells (hiPSCs) and their derivative cell types, MEA recordings hold increasing potential in the study of genetically specific diseases and screening of drug molecules, where the effects and interactions with human cells can already be assessed during the preclinical phase [7]. These cellular models can also be used to study cardiac cells and neural plasticity in developmental stages [2], [8] or regeneration following trauma [9]. The culture times required by human stem cells can differ from studies using rodent cells due to the significantly longer maturation time of human cells [10], which also sets increasing requirements for the stability of MEA structures.

Manuscript received March 4, 2022; revised May 12, 2022; accepted May 15, 2022. Date of publication June 3, 2022; date of current version July 1, 2022. This work was supported by the Academy of Finland under Grant 311017, Grant 311021, Grant 311022, and Grant 336785. The associate editor coordinating the review of this article and approving it for publication was Prof. Irene Taurino. *(Corresponding author: Antti Karttu.)*

This work involved in its research. Approval of all ethical and experimental procedures and protocols was granted by the Faculty of Medicine and Health Technology, Tampere University, has a supportive statement from the Regional Ethics Committee of Pirkanmaa Hospital District for the Derivation, Culture, and Differentiation of hESCs under Approval No. R05116.

Antti Karttu, Jari Väliaho, Jukka Lekkala, and Pasi Kallio are with the Faculty of Medicine and Health Technology, Tampere University, 33720 Tampere, Finland (e-mail: antti.karttu@tuni.fi; jari.valiaho@tuni.fi; jukka.lekkala@tuni.fi; pasi.kallio@tuni.fi).

Kimmo Lahtonen is with the Faculty of Engineering and Natural Sciences, Tampere University, 33720 Tampere, Finland (e-mail: kimmo.lahtonen@tuni.fi).

Juha Heikkilä and Susanna Narkilahti are with the Faculty of Medicine and Health Technology, Tampere University, 33520 Tampere, Finland (e-mail: juha.heikkila@tuni.fi; susanna.narkilahti@tuni.fi).

Digital Object Identifier 10.1109/JSEN.2022.3178640

Although several advancements have been made to the MEA structure and electrode performance, the insulation layer has received very little attention while remaining crucial for the reliability of MEAs. Issues with insulator durability were addressed in the first publication on MEAs by Thomas *et al.* [11], and the importance of the layer was emphasized early by Gross [12]. Problems with insulator stability have been reported with widely used silicon nitride (SiN) fabricated using plasma-enhanced chemical vapor deposition (PECVD) [13], [14]. These findings raise concerns about the longevity of electrical insulation in cell experiments, which can extend to several months or even up to over a year [2], [15]. The reuse of MEAs is a common practice for several subsequent experiments, which further increases the risk of insulator damage in prolonged use. The transmission of electrical activity within the network has a large role in both neuronal and cardiac studies, and in MEA measurements, spatial detection is enabled by precise electrode openings in the insulator. As a requirement for reliable biological conclusions based on the retrieved electrical signals, the insulation layer must perform as intended to prevent the leakage and attenuation [12] of the already weak signals. Extensive damage to insulation may lead to the erroneous pickup of signals outside the intended electrode area, which can easily be interpreted as false network activity during the data analysis.

SiN is routinely applied for encapsulation and passivation in semiconductor and microelectromechanical system (MEMS) fabrication [16], [17]. It is used for scratch protection [18] and is considered as an effective barrier to moisture [16], [17]. However, the typical operating conditions for semiconductors differ significantly from the harsh physiological environment that MEAs are required to endure. Whereas typical electronics may be subjected to water vapor or occasional saline spray, MEAs are exposed to continuous immersion with various ions and enzyme activity at elevated temperature (37 °C) and high humidity. Merely testing the degradation by immersion in saline or buffer solution does not represent the actual conditions during a cell culture, although it may already reveal degradation of the structures. The biological and chemical activity can be strongly dependent on the media used and should be tested with each potential material separately. PECVD SiN films are also prone to small voids in the form of pinholes, which can act as the starting points for corrosion, causing short circuits through the insulator.

Alternative materials for the insulation layer can be used, although compatibility with other parts of the microfabrication process limits the choices available. All structures and materials used must also withstand sterilization. The number of feasible options is further decreased by the need for cytocompatibility with the cultivated cells. Materials that are nontoxic may still lead to adhesion problems with cultured cells, hindering proliferation and network formation. Thin-film ceramics possessing a relatively high dielectric constant - such as SiN or silicon dioxide (SiO_2) - are traditionally used as an insulation layer in MEAs [13], [19]–[23]. Instead of replacing the entire insulation layer with an alternative material, a suitable protection layer can be used to provide the required chemical stability. The use of atomic layer deposition (ALD), for example, enables the fabrication of thin and uniform coatings, which penetrate and seal small voids resulting from the PECVD process.

Here, we bring forward the issue with the wear of PECVD SiN while in contact with cell culture media. We confirmed and quantified the corrosion behavior of both in-house and commercial PECVD SiN in a controlled physiological setting resembling cell culture conditions. A stable insulator alternative by using annealed ALD TiO_2 as a protective layer was developed, tested and compared with the SiN counterpart.

Electrochemical impedance spectroscopy (EIS) was applied in a novel way to study the electrical integrity and thickness changes in the insulation layers when exposed to two cell culture media. Endpoint analysis using profilometry was performed to confirm the actual changes in thickness. A second immersion test was performed on insulators with four different media to monitor the pH of the solutions and wear at the end of the experiment using profilometry. In vitro cytocompatibility of the developed insulator with a transparent ALD TiO_2 protective layer was evaluated by cultivating hESC neuronal cells on the surface for 28 days.

II. Materials and Methods

A. Thickness and Integrity Analysis

EIS was applied as a method for estimating the corrosion rate and film integrity. The measurements can be performed with electrically conductive cell culture media acting as an electrolyte. EIS has been widely used in material sciences and electronics to assess corrosion and dielectric properties on thin films and coatings [24]–[26]. The electrical behavior of the insulation layer can be modeled as a capacitor, where the conductive solution and the electrodes underneath the coating act as parallel plates separated by a layer of dielectric material. The capacitance value is inversely proportional to the layer thickness and can be calculated from the imaginary part of the measured complex impedance spectrum. Deviation of the spectrum from purely capacitive behavior can be used as an indicator of a failed insulator.

The interface between the electrolyte and insulator along with the underlying electrodes can be represented as an electrical equivalent circuit. A model described by Bousse and Bergveld [27] for an insulator-electrolyte interface on a silicon substrate is used here as a starting point (Figure 1a).

An electrical double layer is formed on the insulator when immersed in aqueous solution. C_{DL} represents the double layer capacitance. The capacitance C_a is related to the adsorption of ions at the interface, and Z_w is the Warburg impedance. Z_s is the impedance of the silicon semiconductor, which in this case would be replaced by the metal conductor under the insulator. R_b is the bulk resistance of the electrolyte and Z_{ref} is the impedance of the reference electrode. An insulation layer that is expected to be free of voids and leakage is represented as an ideal capacitance C_i.

An intact MEA insulator can be modeled using this ideal capacitive behavior in a simplified form (Figure 1b). The solution resistance R_s and resistance of the metal conductor R_m are placed in series with the insulator capacitance. The electrical double layer can be modeled as a single capacitance in series with insulator capacitance. Capacitances of 10-40 $\mu F/cm^2$ for double layer have been reported for electrode-electrolyte

interfaces [28], [29]. For a 1-cm^2 electrode area with a 500-nm layer of SiN (dielectric constant 7 [30]), the calculated insulator capacitance is 12 nF with Eq 1. With capacitors connected in series, the smaller value of the insulation layer dominates the total capacitance. As the insulator capacitance is lower than that of the double layer by several orders of magnitude, the measured capacitance is a good representation of the insulation layer, and the double layer capacitance can be omitted.

The capacitance of the insulation layer can be calculated with equation 1, where ε_0 is the vacuum permittivity, ε_r is the relative permittivity (dielectric constant) of the material, A is the area, and d is the distance between capacitor plates.

$$C = \varepsilon_0 \varepsilon_r \frac{A}{d} \tag{1}$$

Because the equivalent circuit for the insulator-electrolyte interface (Figure 1b) contains only resistive and capacitive components, the imaginary part of the complex impedance is solely affected by the capacitance. The impedance of a capacitor Z_c is given in Eq 2, where j is the imaginary unit and ω is the angular frequency. Angular frequency ω equals 2πf, where f is frequency.

$$Z_c = -\frac{1}{j\omega C} \tag{2}$$

Based on Eqs 1 and 2, the insulator impedance is proportional to the thickness of the layer. Corrosion of the insulation layer is detectable with EIS as increased capacitance and lowered impedance. As the frequency at each EIS measurement point is known, the capacitance value can be calculated from the imaginary part of the complex impedance and thickness of an intact insulator using Eq 1, as the dielectric constant and area are known. The measured complex impedance contains information on the resistive and capacitive behavior of the system, which allows the detection of insulator leakage as resistive paths and loss of thickness as increased capacitance. The impedance spectrum of an intact insulator appears primarily as an ideal capacitance with a phase angle of $-90°$, whereas local voids act as resistive paths in parallel and will change the shape of both impedance magnitude and phase angle curves.

A test slide (Figure 2) was designed to mimic the insulated areas of an MEA in a simplified form without the effect of the microelectrode openings. Although the actual microelectrodes were omitted from the structure, the model represents the behavior of an MEA insulator in a cell culture environment. Relatively large circular titanium electrodes were buried under an insulation layer to act similarly to the conducting tracks on an MEA. Electrode diameters were scaled up to allow evaluation of larger insulated areas and increase the measured capacitance. The higher capacitance level allows a lower detection limit for changes in thickness while reducing the effect of stray capacitances of the measurement system. The larger area also increases the likelihood of detecting possible failures or defects. The electrode diameters used were 1.5 mm and 2 mm, with two of each size on the slide. The effective areas were estimated by calculating the conductive area of each electrode and track located inside a 14-mm-diameter circle representing the medium well. The effective areas determined

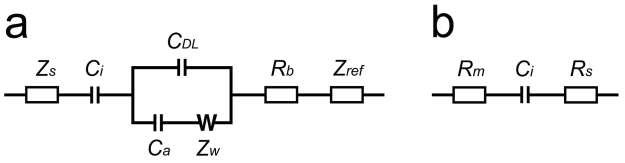

Fig. 1. (a) Equivalent circuit for the interface between a semiconductor, insulator and electrolyte. Redrawn from Bousse and Bergveld [26], [27]. (b) Simplified electrical model for the MEA insulator.

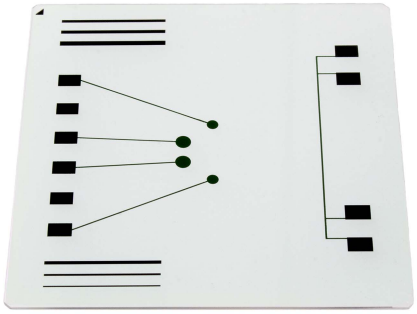

Fig. 2. Test slide with TiO_2 protected insulator.

were 2.43 mm^2 and 3.59 mm^2 for the 1.5 mm and 2 mm electrode diameters, respectively. The capacitance values for silicon nitride were calculated with Eq 1 using a film thickness of 500 nm and dielectric constant of 7. The calculated capacitance values were 301 pF and 445 pF for the 1.5 mm and 2 mm electrodes, respectively.

An impedance spectrum from 100 Hz to 1 MHz was obtained for each insulated electrode with 10 mV sinusoidal input using an IviumStat potentiostat (Ivium Technologies). Electrical connections between a test slide and the potentiostat were established through a commercial MEA head stage frame without amplifier electronics (MEA1060INV-CA from Multi Channel Systems MCS GmbH). A two-electrode configuration was used, with a platinum wire (ALS Co., Ltd) immersed in the medium as the counter electrode, while the titanium electrode under insulation acted as the working electrode. Ten frequencies per decade were measured with a total of 41 sample points for each spectrum. The spectral measurement was repeated three times for each electrode and averaged. For data acquisition, IviumSoft (Ivium Technologies) was used, and the resulting data were analyzed using MATLAB R2019a (MathWorks). The capacitance of the insulator was calculated from the imaginary part of the complex impedance by averaging over three repeated measurements. The frequency range of 200 Hz to 1 kHz was selected for the capacitance analysis.

Contact profilometry was used to physically validate the EIS thickness estimates and evaluate the rate of corrosion in four different cell culture media. A Bruker DektakXT profilometer (Bruker) was used to measure the thickness profile at the inner perimeter of the medium chamber. The transition from the medium exposed area to the surface covered by the PDMS ring was used to determine the possible wear. Thickness change was measured at six points around the perimeter, and the results were averaged over six points.

B. Fabrication of Test Slides

During metal deposition in the electrode fabrication, metal stencils were used as a shadow mask allowing metal patterning

in a single step. Stencils containing the openings for electrodes, conductive tracks and contact pads were laser cut out of a 0.2-mm-thick stainless steel sheet. A conductor width of 200 μm was selected based on the capabilities of the laser cutting process. Before metal deposition, 49 × 49 × 0.7 mm Borofloat 33 glass slides (Schott) were cleaned in an ultrasonic (US) bath with acetone and isopropanol, rinsed with deionized (DI) water and blow-dried with nitrogen. Titanium (400 nm) was deposited on glass slides with electron beam evaporation at 5 Å/s through metal stencil masks using an Orion BC-3000 box coater (System Control Technologies).

All PECVD layers were fabricated with Plasmalab 80 Plus (Oxford Instruments). Three different insulator variations were prepared for testing: SiN deposited at 300 °C, SiN deposited at 400 °C and a SiN-SiO_2-SiN stack coated with ALD TiO_2 – the protected insulator. SiN with 300 °C deposition was previously found to suffer from substantial wear in BrainPhys medium [14]. An increased SiN deposition temperature of 400 °C was included to observe the possible changes in the corrosion properties. The ALD TiO_2 protected insulator was developed with the aim of providing chemical stability for the insulator throughout the test period.

SiN with a nominal thickness of 500 nm was deposited with gas flow rates of 1000 sccm for 2% SiH_4 diluted with N_2 and 30 sccm for NH_3. The radio frequency (RF) power used was 20 W with chamber pressure 1000 mTorr and table temperatures of 300 °C and 400 °C. The actual measured thickness for the SiN films on glass was 500 nm ±30 nm.

The protected insulator was formed using a PECVD deposited stack covered with an ALD TiO_2 layer. SiN (100 nm) was covered with 250 nm SiO_2, which was again topped with 100 nm SiN at 400 °C. The deposition parameters for SiO_2 were 470 sccm SiH_4 flow and 710 sccm N_2O flow with 20 W RF power and 1000 mTorr chamber pressure. SiN was deposited using the same parameters as previously described. The actual measured thickness of the three-layer stack on glass before ALD was 430 nm.

TiO_2 deposition was carried out using a Picosun Sunale ALD R200 Advanced reactor. Tetrakis(dimethylamido) titanium(IV) ($Ti(N(CH_3)_2)_4$, TDMAT, 99%, Strem Chemicals Inc.), DI water, and Ar (99.9999%, Oy AGA Ab) were used as the Ti precursor, O precursor, and carrier/purge/venting gas, respectively. The film growth rate was calibrated by ellipsometry (Rudolph Auto EL III Ellipsometer, Rudolph Research Analytical). The substrate temperature was kept at 200 °C during deposition. The vapor pressure of TDMAT was increased to 3.6 mbar by heating the precursor bubbler to 76 °C, and the precursor gas delivery line was heated to 85 °C to prevent condensation. The water bubbler was sustained at 18 °C by a Peltier element for stability control. The substrate temperature was stabilized for 30 min before starting the deposition. A TiO_2 film thickness of 30 nm was achieved with 804 ALD cycles. The TiO_2 protective layer was air annealed at 450 °C with a ramp up of 30 minutes, followed by 60 minutes at the target temperature allowed to cool down with the oven. The thermal treatment resulted in a visual change from black to transparent.

Contact pad patterning was made with positive resist PR1-2000A1 (Futurrex Inc.), using the same resist layer for insulator openings and the lift-off process of titanium nitride (TiN) coating. Then, 1.5 ml of resist was spin coated on the slides at 1500 rpm for 40 seconds. The insulator openings for contact pads on all slides were made with reactive ion etching (RIE) using Vision 320 RIE (Advanced Vacuum). SF_6 was used for etching all layers with a flow rate of 25 sccm and RF power of 100 W (at 13.56 MHz) at 20 mTorr pressure. TiN (400 nm) was deposited on the slides by using ion beam-assisted deposition (IBAD) [14] immediately following RIE etching to minimize the formation of a native oxide layer on the titanium surface. The surfaces to be coated were Ar etched for two minutes in the metallization chamber. TiN deposition [14] was performed in a N_2/Ar atmosphere at 2 Å/s with an Orion BC-3000 box coater (System Control Technologies) enhanced with a SainTech ST55 ion source (Telemark). The resist remaining from the RIE step prevented adhesion of TiN to the surface of the slide outside the contact pad area and was removed in a lift-off process using a Microposit Remover 1165 (Specialty Electronic Materials) heated to 80 °C with 10-minute sonication.

The medium chambers were formed out of polydimethylsiloxane (PDMS), which was chosen for its elasticity, ease of fabrication and ability to attach to the materials used without additional adhesives. An 8-mm-thick PDMS slab was molded using a two-part silicone mixture Sylgard 184 (Dow Corning Inc.) and punched into cylindrical wells with an inner diameter of 14 mm and an outer diameter of 23 mm. The PDMS rings were manually positioned around the buried electrodes and lightly pressed onto the insulator surface. The rings were reversibly bonded, allowing easy removal after the experiment without damaging the remaining insulator.

Three commercial 60-electrode MEAs featuring PECVD SiN insulation with a nominal thickness of 500 nm were included in the experiment to provide a point of comparison for state-of-the-art device widely in use. Medium wells for the commercial samples were formed by punching four 8-mm-diameter holes on a 30 × 30 × 8 mm PDMS sheet. The formed structures were placed in the center of the MEA, exposing the insulated areas.

C. Test Slide Preparation and Incubation

The insulator testing conditions were chosen to simulate a stem cell culture. The slides were kept in an incubator at 37 °C, 5% CO2 concentration and high humidity. Four different solutions (phosphate buffer solution, neural maintenance medium, BrainPhys and embryoid body medium) were used for the endurance testing of the slides. Phosphate buffer solutions (PBS) are commonly used to characterize and pretreat MEA electrodes and to study their long-term stability, which may also affect the insulator surface depending on the duration of the exposure. Neural maintenance medium (NMM) and BrainPhys were selected to provide references for solutions used in neuronal studies. Embryoid body (EB) medium containing serum was included to provide insight into possible conditions during cardiac cell culture.

The PBS used was Dulbecco's PBS (DPBS) without Mg^{2+} and Ca^{2+} ions (Lonza). NMM is a medium used with neuronal cultures consisting of 1:1 Dulbecco's Modified Eagle Medium/Nutrient Mixture F-12 (DMEM/F-12) with Glutamax

and Neurobasal, 0.5% N2, 1% B27 with Retinoic Acid, 0.5 mM GlutaMAX, 0.5% NEEA, 50 μM 2-mercaptoethanol (all from Thermo Fisher Scientific), 2.5 μg/ml insulin (Sigma-Aldrich) and 0.1% penicillin/streptomycin (Thermo Fisher Scientific). The third solution used was BrainPhys (STEMCELL Technologies) designed for neuronal cultures [31]. The fourth solution was EB medium consisting of knockout DMEM with 20% fetal bovine serum (Lonza), nonessential amino acids and GlutaMAX (Thermo Fisher Scientific). All solutions were supplemented with 1% penicillin-streptomycin (Thermo Fisher Scientific) to reduce the likelihood of microbial contamination.

The experimental setting for corrosion testing was divided into two parts. The first part focused on the EIS method for assessing film integrity and thickness changes of in-house SiN during incubation. The second part expanded the scope by studying commercial MEAs alongside the in-house fabricated films, with two additional media and pH monitoring. During the first 18-day experiment, the EIS curves were recorded while the insulators were exposed to DPBS and NMM, followed by endpoint profilometer measurements. In the second experiment, insulator behavior in DPBS, NMM, BrainPhys and EB media were further assessed by monitoring the medium pH and performing profilometry after 11 days to determine the corrosion rates.

In the first series, each slide was prepared with 1 ml of the test medium pipetted inside the PDMS chamber. The slides were allowed to be stabilized for 30 minutes before the first impedance measurement. Between measurement points, the slides were kept inside a petri dish in an incubator and allowed to acclimate to room temperature for a minimum of 15 minutes before subsequent measurements. Impedance measurements for the insulators were performed three times a week. After each measurement, the medium was changed to mimic the conditions of a cell culture study. The old medium was removed using a syringe and replaced with 1 ml of fresh medium before placing the slides back in the incubator.

The second test series followed the same protocol for medium changes, while the pH of each well was measured before every medium change using a Sentron SI600 (Wellinq). Each slide was removed from the incubator individually and measured immediately. The applied medium volumes for the in-house samples and commercial MEAs were 1 ml and 300 μl, respectively, due to the differing chamber diameters.

After both experiments, all slides were cleaned with 1% Tergazyme detergent solution (Alconox). PDMS wells were removed before immersing the slides in detergent solution for one hour on an orbital shaker. Slides were then rinsed with DI water, acetone, isopropanol, and DI water and blow-dried with nitrogen. Profilometer measurements were performed on all slides after the cleaning procedure.

D. Cell Culture

Three additional slides were fabricated for cell testing. As described earlier, three tested insulator variations were deposited on bare 49 mm $\times$ 49 mm $\times$ 0.7 mm Borofloat 33 glass slides (Schott). A single 49 mm $\times$ 49 mm $\times$ 1 mm soda lime glass slide (Thermo Scientific) was used as a control with no insulation. Each slide was covered with a 40 mm $\times$ 40 mm $\times$ 8 mm PDMS slab containing nine 6-mm-diameter holes to act as culture wells during incubation.

The cytocompatibility evaluation was carried out with human neuronal cells derived from the human embryonic stem cell (hESC) line Regea 08/023 [32]. The Faculty of Medicine and Health Technology, Tampere University, has a supportive statement from the regional ethics committee of Pirkanmaa Hospital District for the derivation, culture, and differentiation of hESCs (R05116).

The cortical neuron differentiation protocol is described in previous research [33]. The slides were coated with 0.05% polyethylenimine and incubated for one hour at room temperature, washed with sterile water three times and coated with 50 μg/ml human recombinant laminin LN521 (Biolamina) at 4 °C overnight. The cells were plated on slides after a 32-day predifferentiation period [33] with a cell density of 80,000 cells per culture well. The cell culture media used was NMM supplemented with brain-derived neural factor (25 μg/ml; 248-BD, R&D Systems), glial cell line-derived neurotropic factor (50 μg/ml; 212-GD, R&D Systems), dibutyryl cyclic-AMP sodium salt (100 mM; D0627, Sigma-Aldrich), and ascorbic acid (200 mM; A5960, Sigma-Aldrich) and was changed three times per week.

The neuronal cell populations were evaluated with immunocytochemical staining after 28 days of culture in slides [33]. The neurons were stained with primary antibodies against β-tubulin III (1:50; A01627, GenScript) and anti-microtubule-associated protein 2 (1:50; MAP-2 + β, AB5622, Millipore), and Alexa Fluor 488 (1:400; A21206, Thermo Fisher) was used as the secondary antibody. The nuclei were stained with 4′,6-diamidino-2-phenylindole (1:5000; DAPI, D9542, Sigma-Aldrich) and Prolong gold (P36931, Thermo Fisher). Cultures were imaged using an Olympus IX51 inverted microscope equipped with an Olympus DP30BW camera (Olympus Corporation).

III. Results and Discussion

The simplified electrical model presented in Figure 1b and the calculated estimate for the insulator capacitance were validated by comparing a simulated impedance spectrum with a measured impedance spectrum. The simulated response of the system was calculated with Eq1 and Eq2 using estimated values for the circuit components as follows. The cell culture media are generally well conducting, with reported values of 14 mS/cm for DPBS [34], 10.69 mS/cm for Neurobasal [35] and 13.8-15.93 mS/cm for DMEM [35], [36]. Based on this, an estimate of 50 Ω was used for R_s. A capacitance value of 500 pF was calculated for C_i using the estimated electrode area. R_m was estimated at 350 Ω, which consists of the resistance of the titanium track as well as the contact resistance of the TiN pad. The superimposition of calculated spectrum on the measurement result (Figure 3a) shows an excellent fit and validates the match between electrical model and the capacitance estimation method successfully. The phase angle remains at $-90°$ at lower frequencies, implying no leakage and allowing thickness estimation from the data between 200 Hz and 1 kHz.

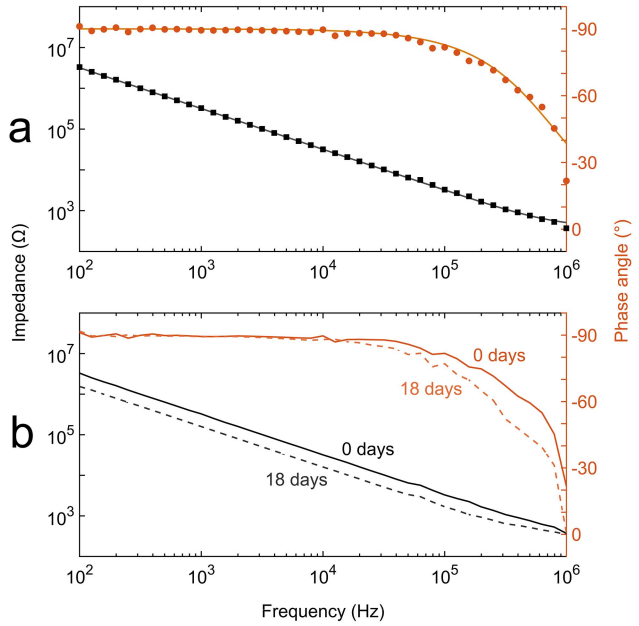

Fig. 3. (a) Measured impedance spectrum (data points) for 2 mm electrode with 300 °C SiN insulation in DPBS after 0 days. Solid lines show the calculated response using the model in Figure 1b with parameters $C_i = 500$ pF, $R_s = 50\ \Omega$ and $R_m = 350\Omega$. (b) EIS curves for the same electrode at 0 and 18 days.

Figure 3b shows the impedances for an electrode in DPBS at the beginning (Day 0) and end (Day 18) of the experiment. The EIS graphs show that the phase angle remains constant at frequencies below 10 kHz, although the impedance magnitude has substantially decreased due to corrosion. The corrosion process is assumed to occur only at the surface and therefore does not affect the dielectric constant of the insulator film. The thickness estimation during the medium exposure was performed based on the relative change, which was used to calculate the change in thickness. This allowed the comparison between different electrode sizes without determining the actual dielectric constant.

In the first experiment series, EIS analysis was performed for 18 test slides over the course of 18 days in DPBS and NMM. Six test slides with three insulator variations (SiN 300 °C, SiN 400 °C and ALD TiO_2 protected SiN) were included, with three slides for each group assessed in DPBS and three in NMM. Every slide contained four electrodes, making up a total of 72 electrodes, as listed in Table I. The impedance spectra on all slides exhibited predominantly capacitive behavior similar to the spectrum presented in Figure 3a which is typical for an intact insulator. No deviation from the capacitive spectrum suggested breakdown of the insulator was recorded during the experiment.

A total of seven electrodes were excluded from the final analysis as outliers due to inconsistencies in the thickness estimate, mostly due to a sudden increase in capacitance after the first measurement, which can be attributed to changes in the surface hydrophilicity. The impedance curves implied an intact film, but the data from the first measurement (Day 0) could no longer be used for accurate estimation of the layer thickness.

The results of the EIS-based thickness assessment in DPBS and NMM are presented in Figure 4 along with the

TABLE I
DESCRIPTION OF THE ELECTRODES USED FOR EIS ANALYSIS IN EXPERIMENT 1

Insulator	Medium	Electrodes measured	Electrodes excluded
SiN 300 °C	DPBS	12	0
	NMM	12	0
SiN 400 °C	DPBS	12	0
	NMM	8	4
ALD TiO_2	DPBS	10	2
	NMM	11	1

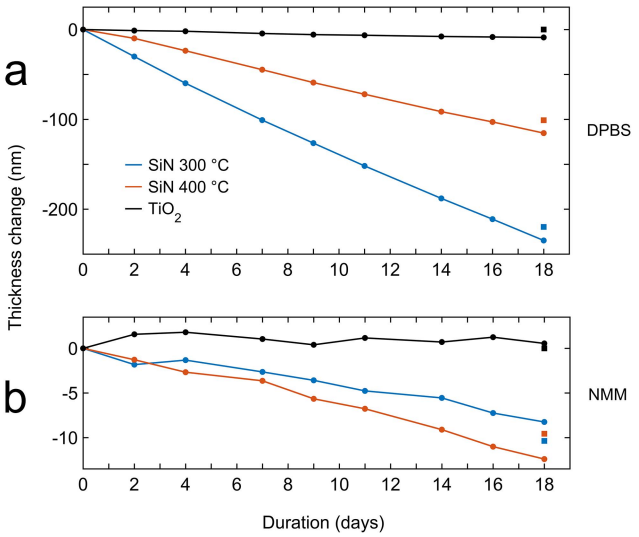

Fig. 4. EIS results for insulator thickness in (a) DPBS and (b) NMM. Squares denote the endpoint profilometer measurements.

profilometer measurements at the endpoint denoted as squares. DPBS resulted in substantial corrosion on the SiN surfaces. Corrosion was observed under a microscope on each slide, and the profilometer measurement confirmed the thickness change at −217.0 nm with SiN 300 °C after 18 days, amounting to 43% of the initial nominal thickness. Increasing the deposition temperature to 400 °C lowered the wear to −101.0 nm. No thickness change was observed with the ALD TiO_2 surface. The thickness change estimated from EIS was −234.8 nm, −115.3 nm and −8.8 nm for SiN 300 °C, SiN 400 °C and TiO_2 protected SiN, respectively.

NMM caused only a slight corrosion for both 300 °C and 400 °C SiN. With both deposition temperatures, a visible edge indicates thickness loss and can be observed under a microscope, even for changes below 10 nm (as shown in Figure 5 with experiment 2). Only a minor difference in the corrosion rate was observed between the two deposition temperatures. Profilometry revealed a decrease of 10.4 nm for 300 °C SiN, while the EIS-based estimate of the thickness change was −8.2 nm. The respective results for 400 °C SiN were −9.5 nm with profilometry and −12.4 nm with EIS. The ALD TiO_2 surfaces exhibited no wear with NMM. No thickness change was indicated under a microscope or through profilometry.

For the ALD TiO_2 surfaces, the EIS data suggest minor thickness changes of less than 10 nm for both media, although no actual change occurred. This can be a result of changes in

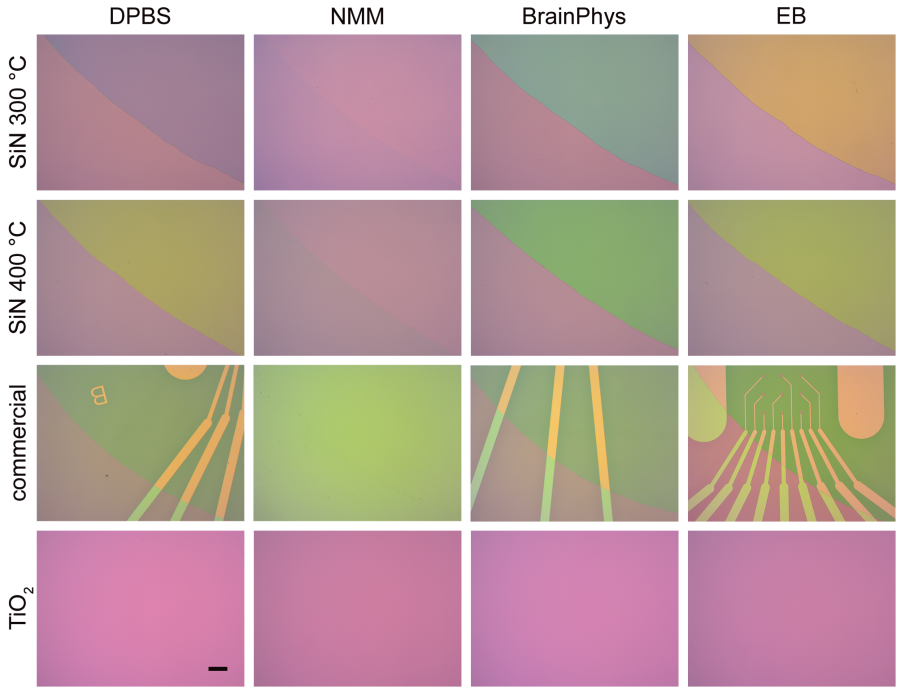

Fig. 5. The effects of media exposure on the insulator surfaces after 11 days imaged using Axio Imager.A1m (Zeiss) (scale bar 200 μm). The bottom left part in each image was covered by a PDMS ring during the experiment.

the surface hydrophilicity or reveal the shortcomings of EIS analysis for tiny capacitance changes. For ten TiO_2 coated electrodes, the capacitance increased noticeably between the first and second measurements, and after the measurement period, the level settled for the remaining data points. This can be considered as insufficient stabilization at the insulator surface after adding the media and not actual wear of the film. For these electrodes, the second measurement point was used as the reference for thickness estimation. These results were included in our analysis, as no corrosion was detected with the profilometer and the capacitance values remained stable after the initial shift.

Compared with the profilometry measurements, the EIS analysis slightly overestimated the thickness reduction for most slides. The difference with the endpoint readings may also be explained by an error in the initial thickness estimate. Calculations using a nominal deposition value and the actual thickness on top of the titanium tracks were not experimentally confirmed. The initial electrode capacitances with SiN ranged from 326 pF to 415 pF for the 1.5 mm electrodes and from 470 pF to 580 pF for the 2 mm electrodes. These conditions provide higher thickness values than the calculated capacitance estimates, which may indicate a thinner initial layer than the expected nominal value. The variation in the initial capacitances is partly explained by the manual positioning of the PDMS rings, which affects the effective electrode area. The capacitances for TiO_2-coated surfaces varied from 265 pF to 287 pF for the 1.5 mm electrodes and from 380 pF to 410 pF for the 2 mm electrodes. This indicates that the ALD-coated stack provides a higher insulation impedance with smaller film thickness, meaning lower signal losses with cellular recordings [12].

Based on these results, EIS analysis acts as a powerful tool for detecting thickness changes for MEA insulator testing.

TABLE II
RESULTS OF EIS AND PROFILOMETER ANALYSIS IN EXPERIMENT 1 (18 DAYS)

Medium	Insulator	Thickness change (nm) EIS	Profilometer	St Dev	Rate (nm/day)
DPBS	SiN 300 °C	-234.8	-217.0	10.2	-12.1
	SiN 400 °C	-115.3	-101.0	4.8	-5.6
	TiO2	-8.8	0	-	0
NMM	SiN 300 °C	-8.2	-10.4	1.3	-0.6
	SiN 400 °C	-12.4	-9.5	2.1	-0.5
	TiO2	0.6	0	-	0

The highly linear wear curves support the assumption that corrosion with SiN occurs at the surface, gradually dissolving the insulator in the medium without affecting the bulk structure of the film. Porosity or localized defects reaching through the insulator would show resistive behavior through the film, which was not observed in the experimental data.

The second series expanded the scope by including a commercial MEA, pH measurement and medium testing with BrainPhys and EB medium supplemented with FBS, both of which have previously been used with SiN insulated MEAs [14], [37]. Corrosion rates for all four media were estimated. Three test slides for each insulator variant and three commercial MEAs were exposed to each of the media and measured. The endpoint thickness changes, calculated corrosion rates and pH recordings are presented in Table II.

Figure 5 clearly shows the corroded edge on all samples except those featuring the TiO_2 protection and NMM with the commercial MEA. On the commercial MEA, NMM showed

TABLE III
PROFILOMETER AND pH MEASUREMENT RESULTS FOR EXPERIMENT 2 (11 DAYS)

Medium	Insulator	Thickness change (nm) Profilometer	StDev	Rate (nm/day)	pH
DPBS	SiN 300 °C	-133.7	7.6	-12.2	6.6
	SiN 400 °C	-59.2	4.8	-5.4	
	commercial	-45.9	2.8	-4.2	
	TiO_2	0	-	0	
NMM	SiN 300 °C	-9.5	1.1	-0.8	7.4
	SiN 400 °C	-9.6	1.0	-0.9	
	commercial	-	-	-	
	TiO_2	0	-	0	
BrainPhys	SiN 300 °C	-245.9	5.2	-22.4	7.5
	SiN 400 °C	-96.3	4.0	-8.8	
	commercial	-69.6	8.1	-6.3	
	TiO_2	0	-	0	
EB	SiN 300 °C	-175.2	3.7	-15.9	7.4
	SiN 400 °C	-71.1	2.9	-6.5	
	commercial	-56.3	2.8	-5.1	
	TiO_2	0	-	0	

faint marks on the edge of PDMS, but the thickness change could not be reliably detected with profilometry after the immersion period. The corrosion rates of in-house SiN with DPBS and NMM confirmed the rates found in the first test series. Commercial MEAs exhibited noticeable wear in DPBS, at 22% lower rate than the in-house 400 °C SiN, likely due to different process parameters and equipment. Herrera-Morales previously obtained a corrosion rate of 2.1 nm/day for 400 °C SiN in PBS [37], [38], although using different deposition parameters and equipment. The tests were performed on a hot plate, differing on incubator conditions regarding humidity and CO_2 levels, with medium changes only once a week.

Here, the introduction of BrainPhys and EB medium revealed more severe degradation on the in-house SiN surfaces when compared to degradation caused by DPBS or NMM. Exposure of SiN 300 °C to BrainPhys for 11 days resulted in a loss of 49% of the nominal insulator thickness. This is in line with previous findings [14], where BrainPhys was able to dissolve most of the insulation layer during a single cell culture cycle. The commercial MEAs exhibited substantial corrosion with both BrainPhys and EB medium. Compared to the in-house 400 °C SiN, the corrosion rates for the commercial MEAs were 28% lower for BrainPhys and 21% lower for EB medium, respectively.

No corrosion was detected with TiO_2 for any of the solutions, suggesting excellent corrosion protection for a wide range of cell culture media.

In each medium, the pH values remained constant throughout the experiment regardless of the possible wear, indicating no direct relation between the pH level and the corrosion rate. DPBS is not buffered to be used in a 5% CO_2 atmosphere, which explains the lower pH in the incubator conditions. NMM, BrainPhys and EB have approximately the same pH, although their corrosion profiles are distinctively different.

The differences in corrosion rates underline the need for systematic testing of MEA materials with different culture media. In the worst case presented here with 300 °C SiN and BrainPhys, the entire 500-nm insulation layer is estimated to be dissolved in under 23 days, which is shorter than the duration of many neuronal studies. With the EB medium used in cardiac studies, the corresponding estimate is 32 days. These estimates do not even take into account the case where signals may already be picked up through the thinned-out insulator once the impedance through the film is low enough.

Increasing the deposition temperature for SiN from 300 °C to 400 °C can reduce the corrosion up to 60%, although the wear is still substantial for several solutions. According to the results within this work, the base medium for NMM appears to be safe for use with SiN, but the effects of possible supplements are not assessed.

The commercial MEAs showed slightly improved stability over the in-house 400 °C SiN, for which however the other deposition parameters were not optimized. Nevertheless, the commercial MEAs were also subject to substantial corrosion with several cell culture media during a relatively short observation period. The results here suggest that the nominal insulation thickness of 500 nm is lost entirely after 80 days in contact with BrainPhys, which can be exceeded when reusing MEAs.

Previous accounts of SiN insulator corrosion [14] and cracking [13] have been reported, but the severity of the problem has not been properly addressed in the literature, although MEAs with SiN insulation have been in commercial and academic use for decades. Insulation loss can be critical when studying the electrical stimulation of cultured cells, where leakages of up to 30% of the stimulation current have been reported with a damaged SiN insulator [13]. The lack of insulation outside the electrode sites can lead to the loss of spatial information, as the signal paths for the stimuli or cell activity are no longer well known. A reduction in insulation impedance also causes severe attenuation of the measured signals at electrodes, as described by Gross [12]. With cardiac cells, the effect of insulator leakage may be emphasized due to the higher amplitude of electrical signals compared to neuronal cultures.

The effects of corrosion may be overlooked if the culture chambers are permanently bonded and not removed to observe the signs of possible thickness reduction. The phenomenon is also difficult to detect electrically from a used MEA, as impedance measurements of the opened electrodes do not directly reveal the state of the insulation layer. Although the reduced insulation should lower the measured impedance, the TiN electrodes increase in impedance [14] over time due to oxidation, potentially counteracting and masking the effect of insulation loss on the measurement.

Dissolution of SiN in aqueous media has been reported with powder and PECVD thin films [39], [40], along with

studies related to implantable hip joint replacements [18], [41]. Dissolution of SiN has been found to be linear and occurs at the surface [42], which supports the results here. The dissolution process has been suggested to occur first by hydrolysis at the SiN surface through reaction

$$Si_3N_4 + 6H_2O \leftrightarrow 3\ SiO_2 + 4\ NH_3 \tag{3}$$

where exposure to water partly oxidizes the surface, forming SiO_2 and ammonia [39], [42]–[44]. The oxidized surface is further dissolved through reaction

$$SiO_2 + 2\ H_2O \leftrightarrow Si(OH)_4 \tag{4}$$

producing silicic acid. It is worth noting that PECVD SiN films are nonstoichiometric, containing varying rates of hydrogen from the gas precursor, both of which may affect the dissolution properties. The film properties can vary significantly depending on the deposition parameters, including gas flow rates, temperature and RF power, as well as the equipment used. Here, only the effect of increased deposition temperature was demonstrated. Although the culture media is buffered for pH, the presence of the released reaction products may affect the cells locally at the corroding surface. Frequent changes of the culture medium also prevent the solution from saturating with reaction products, allowing corrosion to proceed for the duration of the culture. To ensure a consistent insulation performance throughout the cell culture period, a more chemically stable coating can be applied, as shown here. ALD TiO_2 layers have been applied for biological studies by Herrera-Morales [38] and more recently by Dollt *et al.* [45]. In the latter, the approach was to form an insulating coating over the electrodes, which we did not see as beneficial due to the increased electrode impedance levels. Here, the proposed method applies a protective layer covering only the insulator by eliminating the coating at the measurement sites. This method is compatible with existing MEA fabrication methods [14], [21], [46], where the TiO_2 layer would be etched over the electrodes together with the underlying dielectric layers before applying the final electrode surface.

TiO_2 resulting from the ALD process is initially black and moderately conductive, both of which are undesirable qualities when protecting the electrical insulator in cell studies. The opaqueness and conductance can, however, be counteracted by air annealing. The major benefits of annealed TiO_2 used here include vastly improved optical transparency, allowing the use of traditional optical microscopy methods needed in cell studies, reduced electrical conductivity of the protective layer and increased chemical stability of the surface. The effects of thermal annealing on the optical transparency and reduction in electrical conductivity of ALD TiO_2 have been described by Ali-Löytty *et al.* [47]. This is attributed to the transformation from the amorphous phase to more stable crystalline rutile that is achieved through oxidation at temperatures above 200 °C. Increased chemical stability in NaOH was also reported with air annealing at 300 °C or higher [47].

Although the annealed ALD TiO_2 alone does not provide sufficient electrical insulation, coating on thin film ceramics can be tailored to surpass the performance of a single SiN layer. Here, a layer of SiO_2 featuring a low dielectric constant was sandwiched between two SiN layers to provide higher insulation impedance and to eliminate residual stress in the deposited layer. The ALD TiO_2 layer seals possible pinholes in the SiN surface, which may otherwise serve as starting points for corrosion and electrical short circuits. SiN underneath the protective ALD TiO_2 layer provides a diffusion barrier for ions, which SiO_2 alone is not capable of. This layered structure provides lower capacitance and losses with the same film thickness compared to SiN while remaining stable in various cellular media.

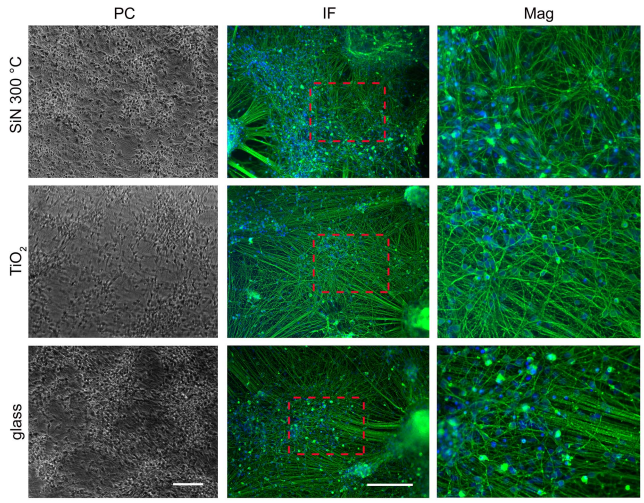

Fig. 6. Cultured in vitro hESC neurons for cytocompatibility evaluation. Phase contrast images (PCs) were taken 7 days after plating the cells. Magnification 10× using Zeiss Axio Observer A1 (Zeiss). Immunofluorescence images (IFs) were taken after fixing the cells at 28 days. The labels used were DAPI in the blue channel for cell nuclei and MAP-2 + β-tubulin in the green channel for neuronal cells. Magnification 10× using Olympus IX-51. Digital magnifications of immunofluorescence images (Mag) are from the dashed line areas. Scale bar represents 200 μm in each image.

A. Cytocompatibility of ALD TiO_2

The cytocompatibility of the ALD TiO_2 surface was evaluated using hESC-derived neurons. Cell growth and viability were visually inspected once per week during the experiment. All sample groups (300 °C SiN, ALD TiO_2-coated SiN and glass substrates) exhibited similar growth rates and good viability throughout the culture period. At later timepoints, the cell growth aggregated to some extent in all samples, as shown in immunofluorescence images (IF) in Figure 6. Immunocytochemical staining after 28 days showed similar dense neuronal networks with each sample group regardless of the surface coating type. The developed ALD TiO_2 insulator appeared to promote neuronal cell growth with no signs of cytotoxicity. The cell visibility with ALD TiO_2 during microscopy was comparable to that of SiN-coated glass and a plain microscope slide. According to the results of the cytocompatibility evaluation, the ALD TiO_2 protected insulator suggested herein could be directly implemented in MEA measurements without adverse effects on neuronal cell viability or microscopy.

IV. Conclusion

The possibility of degradation with SiN insulation should be considered as a potential source of error in MEA recordings. SiN degradation potentially affects the reliability and analysis

of MEA measurements in cellular electrophysiology studies due to loss of electrical insulation. The quality of the recordings can be compromised, especially when reusing MEAs for subsequent experiments, where the exposure time to the media is prolonged. Here, we addressed the severity of SiN corrosion with select cell culture media by using both in-house deposited coatings and commercial MEAs. The findings in this paper raise serious concerns about the effects of this phenomenon on the results of previously performed experiments with extended culture periods and reuse of MEAs.

EIS measurements were successfully introduced as the means of monitoring the insulator film thickness and integrity in the media during incubation, showing linear corrosion behavior on the in-house SiN surfaces. The measurement method presented here can be applied for the screening of insulator materials and their possible quantitative degradation in culture conditions. The alarming corrosion rates of in-house and commercial SiN surfaces with certain typically used media call for the re-evaluation of MEA insulators widely in use. All SiN films studied in this paper showed varying degrees of wear depending on the media used, with no direct relation to the pH. The corrosion reaction mechanisms between the surface and medium are not well understood due to the complex composition of both the cell culture media and PECVD SiN, warranting further research. The consequences of insulation loss should also be studied in more detail at the signal level.

The ALD TiO_2 protected insulator was developed to address the need for a more reliable MEA insulator for long-term measurements. The featured ALD coating was found to entirely prevent corrosion in this setting while showing good in vitro cytocompatibility with hESC-derived neurons. Both the chemical stability and electrical impedance of the developed corrosion-protected insulator were found to surpass the features of those with a single SiN layer. The proposed fabrication method can be used to directly replace the traditional SiN insulator, providing increased reliability for sensors used in electrophysiological studies while allowing the same optical imaging methods to be used. The proposed insulator structure provides improved overall performance without requiring any changes in culture or measurement protocols from the end user. The described protective layer may also provide benefits to other applications where chemical stability in biological fluids is needed.

REFERENCES

[1] E. Cotterill, D. Hall, K. Wallace, W. R. Mundy, S. J. Eglen, and T. J. Shafer, "Characterization of early cortical neural network development in multiwell microelectrode array plates," *J. Biomol. Screening*, vol. 21, no. 5, pp. 510–519, Jun. 2016, doi: 10.1177/1087057116640520.

[2] A. Odawara, H. Katoh, N. Matsuda, and I. Suzuki, "Physiological maturation and drug responses of human induced pluripotent stem cell-derived cortical neuronal networks in long-term culture," *Sci. Rep.*, vol. 6, no. 1, p. 26181, May 2016, doi: 10.1038/srep26181.

[3] E. J. MacLaren, P. Charlesworth, M. P. Coba, and S. G. N. Grant, "Knockdown of mental disorder susceptibility genes disrupts neuronal network physiology *in vitro*," *Mol. Cellular Neurosci.*, vol. 47, no. 2, pp. 93–99, Jun. 2011, doi: 10.1016/j.mcn.2010.12.014.

[4] A. F. M. Johnstone, G. W. Gross, D. G. Weiss, O. H.-U. Schroeder, A. Gramowski, and T. J. Shafer, "Microelectrode arrays: A physiologically based neurotoxicity testing platform for the 21st century," *NeuroToxicology*, vol. 31, no. 4, pp. 331–350, Aug. 2010, doi: 10.1016/j.neuro.2010.04.001.

[5] L. Ylä-Outinen, "Human cell-based micro electrode array platform for studying neurotoxicity," *Frontiers Neuroeng.*, vol. 3, p. 111, Sep. 2010, doi: 10.3389/fneng.2010.00111.

[6] E. G. Navarrete *et al.*, "Screening drug-induced arrhythmia using human induced pluripotent stem cell–derived cardiomyocytes and low-impedance microelectrode arrays," *Circulation*, vol. 128, no. 11, pp. S3–S13, Sep. 2013, doi: 10.1161/CIRCULATIONAHA.112.000570.

[7] S. Kussauer, R. David, and H. Lemcke, "hiPSCs derived cardiac cells for drug and toxicity screening and disease modeling: What microelectrode-array analyses can tell U.S.," *Cells*, vol. 8, no. 11, Oct. 2019, Art. no. 1331, doi: 10.3390/cells8111331.

[8] T. J. Heikkilä *et al.*, "Human embryonic stem cell-derived neuronal cells form spontaneously active neuronal networks *in vitro*," *Exp. Neurol.*, vol. 218, no. 1, pp. 109–116, Jul. 2009, doi: 10.1016/j.expneurol.2009.04.011.

[9] M. Häkli *et al.*, "Human induced pluripotent stem cell-based platform for modeling cardiac ischemia," *Sci. Rep.*, vol. 11, no. 1, p. 4153, Feb. 2021, doi: 10.1038/s41598-021-83740-w.

[10] P. Lu *et al.*, "Prolonged human neural stem cell maturation supports recovery in injured rodent CNS," *J. Clin. Invest.*, vol. 127, no. 9, pp. 3287–3299, Sep. 2017, doi: 10.1172/JCI92955.

[11] C. A. Thomas, P. A. Springer, G. E. Loeb, Y. Berwald-Netter, and L. M. Okun, "A miniature microelectrode array to monitor the bioelectric activity of cultured cells," *Express Cell. Res.*, vol. 74, no. 1, pp. 61–66, Sep. 1972, doi: 10.1016/0014-4827(72)90481-8.

[12] G. W. Gross, "Simultaneous single unit recording *in vitro* with a photoetched laser deinsulated gold multimicroelectrode surface," *IEEE Trans. Biomed. Eng.*, vol. BME-26, no. 5, pp. 273–279, May 1979, doi: 10.1109/TBME.1979.326402.

[13] D. A. Wagenaar, J. Pine, and S. M. Potter, "Effective parameters for stimulation of dissociated cultures using multi-electrode arrays," *J. Neurosci. Methods*, vol. 138, nos. 1–2, pp. 27–37, 2004, doi: 10.1016/j.jneumeth.2004.03.005.

[14] T. Ryynänen, M. Toivanen, T. Salminen, L. Ylä-Outinen, S. Narkilahti, and J. Lekkala, "Ion beam assisted E-beam deposited TiN microelectrodes—Applied to neuronal cell culture medium evaluation," *Frontiers Neurosci.*, vol. 12, p. 882, Dec. 2018, doi: 10.3389/fnins.2018.00882.

[15] S. M. Potter and T. B. DeMarse, "A new approach to neural cell culture for long-term studies," *J. Neurosci. Methods*, vol. 110, nos. 1–2, pp. 17–24, Sep. 2001, doi: 10.1016/s0165-0270(01)00412-5.

[16] A. E. Kaloyeros, F. A. Jové, J. Goff, and B. Arkles, "Silicon nitride and silicon nitride-rich thin film technologies: Trends in deposition techniques and related applications," *ECS J. Solid State Sci. Technol.*, vol. 6, no. 10, pp. 691–714, Sep. 2017, doi: 10.1149/2.0011710jss.

[17] A. E. Kaloyeros, F. A. Jové, J. Goff, and B. Arkles, "Silicon nitride and silicon nitride-rich thin film technologies: State-of-the-art processing technologies, properties, and applications," *ECS J. Solid State Sci. Technol.*, vol. 9, no. 6, Aug. 2020, Art. no. 063006, doi: 10.1149/2162-8777/aba447.

[18] J. Olofsson, T. M. Grehk, T. Berlind, C. Persson, S. Jacobson, and H. Engqvist, "Evaluation of silicon nitride as a wear resistant and resorbable alternative for total hip joint replacement," *Biomatter*, vol. 2, no. 2, pp. 94–102, Apr. 2012, doi: 10.4161/biom.20710.

[19] H. Hämmerle, U. Egert, A. Mohr, and W. Nisch, "Extracellular recording in neuronal networks with substrate integrated microelectrode arrays," *Biosensors Bioelectron.*, vol. 9, nos. 9–10, pp. 691–696, Feb. 1994, doi: 10.1016/0956-5663(94)80067-7.

[20] W. Nisch, J. Böck, U. Egert, H. H. Mmerle, and A. Mohr, "A thin film microelectrode array for monitoring extracellular neuronal activity *in vitro*," *Biosensors Bioelectron.*, vol. 9, nos. 9–10, pp. 737–741, Feb. 1994, doi: 10.1016/0956-5663(94)80072-3.PMID:7695849.

[21] U. Egert *et al.*, "A novel organotypic long-term culture of the rat hippocampus on substrate-integrated multielectrode arrays," *Brain Res. Protocols*, vol. 2, no. 4, pp. 229–242, Jun. 1998, doi: 10.1016/s1385-299x(98)00013-0.

[22] J. Pine, "Recording action potentials from cultured neurons with extracellular microcircuit electrodes," *J. Neurosci. Methods*, vol. 2, no. 1, pp. 19–31, Feb. 1980, doi: 10.1016/0165-0270(80)90042-4.

[23] S. B. Jun *et al.*, "Low-density neuronal networks cultured using patterned poly-l-lysine on microelectrode arrays," *J. Neurosci. Methods*, vol. 160, no. 2, pp. 317–326, Mar. 2007, doi: 10.1016/j.jneumeth.2006.09.009.

[24] J. Colreavy and J. D. Scantlebury, "Electrochemical impedance spectroscopy to monitor the influence of surface preparation on the corrosion characteristics of mild steel MAG welds," *J. Mater. Process. Technol.*, vol. 55, nos. 3–4, pp. 206–212, Dec. 1995, doi: 10.1016/0924-0136(95)01955-3.

[25] V. B. Mišković-Stankovič, D. M. Dražić, and M. J. Teodorović, "Electrolyte penetration through epoxy coatings electrodeposited on steel," *Corrosion Sci.*, vol. 37, no. 2, pp. 241–252, Feb. 1995, doi: 10.1016/0010-938x(94)00130-x.

[26] F. Deflorian, L. Fedrizzi, S. Rossi, and P. L. Bonora, "Organic coating capacitance measurement by EIS: Ideal and actual trends," *Electrochim. Acta*, vol. 44, no. 24, pp. 4243–4249, Jul. 1999, doi: 10.1016/s0013-4686(99)00139-5.

[27] L. Bousse and P. Bergveld, "On the impedance of the silicon dioxide/electrolyte interface," *J. Electroanal. Chem. Interfacial Electrochem.*, vol. 152, nos. 1–2, pp. 25–39, Aug. 1983, doi: 10.1016/S0022-0728(83)80030-8.

[28] D. A. Robinson, "The electrical properties of metal microelectrodes," *Proc. IEEE*, vol. 56, no. 6, pp. 1065–1071, Jun. 1968, doi: 10.1109/PROC.1968.6458.

[29] A. Hassibi, R. Navid, R. W. Dutton, and T. H. Lee, "Comprehensive study of noise processes in electrode electrolyte interfaces," *J. Appl. Phys.*, vol. 96, no. 2, pp. 1074–1082, Jul. 2004, doi: 10.1063/1.1755429.

[30] A. Piccirillo and A. L. Gobbi, "Physical-electrical properties of silicon nitride deposited by PECVD on III–V semiconductors," *J. Electrochem. Soc.*, vol. 137, no. 12, pp. 3910–3917, Dec. 1990, doi: 10.1149/1.2086326.

[31] C. Bardy *et al.*, "Neuronal medium that supports basic synaptic functions and activity of human neurons *in vitro*," *Proc. Nat. Acad. Sci. USA*, vol. 112, no. 20, Apr. 2015, doi: 10.1073/pnas.1504393112.

[32] H. Skottman, "Derivation and characterization of three new human embryonic stem cell lines in Finland," *Vitro Cellular Develop. Biol.-Animal*, vol. 46, nos. 3–4, pp. 206–209, Feb. 2010, doi: 10.1007/s11626-010-9286-2.

[33] T. Hyvärinen *et al.*, "Functional characterization of human pluripotent stem cell-derived cortical networks differentiated on laminin-521 substrate: Comparison to rat cortical cultures," *Sci. Rep.*, vol. 9, no. 1, Nov. 2019, doi: 10.1038/s41598-019-53647-8.

[34] G. Fuhr, H. Glasser, T. Müller, and T. Schnelle, "Cell manipulation and cultivation under ac electric field influence in highly conductive culture media," *Biochim. Biophys. Acta*, vol. 1201, no. 3, pp. 353–360, Dec. 1994, doi: 10.1016/0304-4165(94)90062-0.

[35] J. Hurst *et al.*, "Comparison of different cell culture media in the model of the isolated and superfused bovine retina: Investigating the limits of more physiological perfusion solutions," *Current Eye Res.*, vol. 43, no. 2, pp. 232–243, Nov. 2017, doi: 10.1080/02713683.2017.1387668.

[36] G. Fuhr *et al.*, "Radio-frequency microtools for particle and liver cell manipulation," *Sci. Nat.*, vol. 81, no. 12, pp. 528–535, Dec. 1994, doi: 10.1007/BF01139998.

[37] T. Ryynänen *et al.*, "Microelectrode array for noninvasive analysis of cardiomyocytes at the single-cell level," *Jpn. J. Appl. Phys.*, vol. 57, no. 11, Nov. 2018, Art. no. 117001, doi: 10.7567/jjap.57.117001.

[38] J. M. H. Morales, "Evaluating biocompatible barrier films as encapsulants of medical micro devices," Ph.D. dissertation, Dept. Mater. Univ. Grenoble-Alpes, Grenoble, France, 2015.

[39] E. Laarz, B. V. Zhmud, and L. Bergström, "Dissolution and deagglomeration of silicon nitride in aqueous medium," *J. Amer. Ceram. Soc.*, vol. 83, no. 10, pp. 2394–2400, Dec. 2004, doi: 10.1111/j.1151-2916.2000.tb01567.x.

[40] S.-K. Kang *et al.*, "Dissolution behaviors and applications of silicon oxides and nitrides in transient electronics," *Adv. Funct. Mater.*, vol. 24, no. 28, pp. 4427–4434, Jul. 2014, doi: 10.1002/adfm.201304293.

[41] M. Pettersson *et al.*, "Dissolution behaviour of silicon nitride coatings for joint replacements," *Mater. Sci. Eng., C*, vol. 62, pp. 497–505, May 2016, doi: 10.1016/j.msec.2016.01.049.

[42] J. N. Chiang, S. G. Ghanayem, and D. W. Hess, "Low-temperature hydrolysis (oxidation) of plasma-deposited silicon nitride films," *Chem. Mater.*, vol. 1, no. 2, pp. 194–198, 1989, doi: 10.1021/cm00002a006.

[43] J. W. Osenbach and W. R. Knolle, "Behavior of a-SiN: H and a-SiON: H films in condensed water," *J. Electrochem. Soc.*, vol. 139, no. 11, pp. 3346–3351, Nov. 1992, doi: 10.1149/1.2069076.

[44] B. V. Zhmud and L. Bergström, "Dissolution kinetics of silicon nitride in aqueous suspension," *J. Colloid Interface Sci.*, vol. 218, no. 2, pp. 582–584, Oct. 1999, doi: 10.1006/jcis.1999.6425.

[45] M. Dollt *et al.*, "Low-temperature atomic layer deposited oxide on titanium nitride electrodes enables culture and physiological recording of electrogenic cells," *Frontiers Neurosci.*, vol. 14, Sep. 2020, Art. no. 552876, doi: 10.3389/fnins.2020.552876.

[46] M. Janders, U. Egert, M. Stelzle, and W. Nisch, "Novel thin film titanium nitride micro-electrodes with excellent charge transfer capability for cell stimulation and sensing applications," in *Proc. 18th Annu. Int. Conf. IEEE Eng. Med. Biol. Soc.*, vol. 1, Jan. 1996, doi: 10.1109/IEMBS.1996.656936.

[47] H. Ali-Löytty *et al.*, "Diversity of TiO_2: Controlling the molecular and electronic structure of atomic-layer-deposited black TiO_2," *ACS Appl. Mater. Interface*, vol. 11, no. 3, pp. 2758–2762, Jan. 2019, doi: 10.1021/acsami.8b20608.